IEEE Access
Multidisciplinary ⋮ Rapid Review ⋮ Open Access Journal

Received 29 January 2024, accepted 18 February 2024, date of publication 20 February 2024, date of current version 26 February 2024.

Digital Object Identifier 10.1109/ACCESS.2024.3367998

RESEARCH ARTICLE

Transparent and Flexible Chessboard Metasurface Based on Optimized Multielement Phase Cancellation for Wideband RCS Reduction

QI CHANG, JINZU JI, AND YUNPENG MA
School of Aeronautic Science and Engineering, Beihang University, Beijing 100191, China
Corresponding author: Yunpeng Ma (ma_yun_peng@126.com)

ABSTRACT An optically transparent chessboard metasurface is proposed to achieve wideband radar cross section (RCS) reduction in this paper. The metasurface is a single-layer sandwich structure composed of indium-tin-oxide (ITO) square patches with different sizes and surface resistances, polyethylene terephthalate (PET) substrate, and ITO backplane from the top downwards. Based on optimized multielement phase cancellation (OMEPC) to select the sizes and surface resistances of ITO patches, the proposed metasurface can achieve the 10 dB RCS reduction from 10.1 to 26.4 GHz with a relative bandwidth of 89% under normal incidence. The total thickness of the metasurface is 2 mm, which makes it highly flexible. When there is a slight cylindrical curvature on the metasurface and the curvature angle is less than 30°, an approximate 10 dB RCS reduction can still be achieved in the frequency range of 10-25 GHz under normal incidence. When the oblique incidence angle is less than 45°, the proposed metasurface also exhibits nearly 10 dB RCS reduction at the specular direction in the frequency range of 10-25 GHz. Finally, a sample is fabricated and measured, and the experimental results are in good agreement with the simulation results.

INDEX TERMS Chessboard metasurface, optimized multielement phase cancellation (OMEPC), radar cross section (RCS) reduction, transparent, flexible.

I. INTRODUCTION

The development of radar detection technology has brought great challenges to the survivability of military targets, so the wideband radar cross section (RCS) reduction of targets has become crucial. Traditional methods mainly achieve RCS reduction by altering the shape or using radar absorbing materials (RAMs). However, altering the shape often results in a deterioration of the aerodynamic performance of targets, and RAM has the disadvantage of being too thick or having a narrow absorption bandwidth [1], [2], [3], [4].

Metasurface has the flexible ability to control electromagnetic (EM) waves, and therefore has good potential prospects in wideband RCS reduction. Metasurfaces can regulate the scattering field through absorption, polarization transformation and phase interference [5], [6], [7], [8]. As metasurfaces are usually very thin, it is difficult to achieve broadband RCS reduction through absorption [9], [10]. Recently, polarization conversion metasurfaces are introduced for RCS reduction [11], [12], [13]. The reduction effect of RCS depends on the polarization conversion rate of the unit cell. However, it is difficult to obtain a metasurface with broadband polarization conversion rate, and the polarization conversion rate is sensitive to the incident angle and polarization mode [14], [15], [16], [17]. Based on the principle of phase interference, metasurfaces containing different artificial magnetic conductors (AMCs) arranged in chessboard configurations have been extensively studied to achieve 10 dB RCS reduction [18], [19], [20]. The most common method is to use two types of AMC elements and make their reflected phase difference close to 180°, and many chessboard metasurface structures have been designed by this method [21], [22], [23], [24], [25]. This method can scatter the incident wave into four main reflection lobes that

The associate editor coordinating the review of this manuscript and approving it for publication was Davide Comite.

© 2024 The Authors. This work is licensed under a Creative Commons Attribution-NonCommercial-NoDerivatives 4.0 License.
For more information, see https://creativecommons.org/licenses/by-nc-nd/4.0/

deviate from the incident direction. Random and encoded metasurfaces have also been introduced, and significant RCS reduction in all directions can be achieved through efficient optimization algorithms [26], [27], [28]. To further improve the RCS reduction bandwidth, the optimized multielement phase cancellation (OMEPC) technique is used for the design of chessboard metasurfaces [29]. This method is achieved by optimizing the shape and size of the unit cells that make up the metasurface, resulting in a wideband reflection phase cancellation on the metasurface. Su et al. proposed the OMEPC method and designed a chessboard metasurface, which can achieve 10 dB RCS reduction in the frequency range of 5.5-32.3 GHz by optimizing the size and thickness of unit cells [30]. Qu et al. designed a chessboard metasurface based on OMEPC, which exhibits 10 dB RCS reduction in a superwide frequency band from 7.4 to 64.8 GHz while maintaining good oblique incidence stability [31].

Most of the reported chessboard metasurfaces are composed of metal patches and substrates. For some special applications such as aircraft cabin that require optical transparency, the reported metasurfaces are difficult to meet the requirements. In addition, these metasurfaces are often inflexible and difficult to apply to RCS reduction for complex targets. To solve this problem, many metamaterial absorbers have been developed based on transparent resistance films such as indium-tin-oxide (ITO) and graphene [32], [33], [34]. Zhang et al. proposed a graphene-based transparent metasurface, which has a 90% absorption effect at 7-18 GHz [35]. Xi et al. designed a transparent double-layer metasurface based on ITO, which utilizes a hybrid mechanism to achieve 10 dB RCS reduction in the frequency band of 7.5-32.2 GHz [36]. Although these proposed transparent metamaterial absorbers have good performance, these absorbers are generally multi-layer structures with large thickness, which limits their practical applications.

In this paper, we apply ITO and polyethylene terephthalate (PET) to the design of transparent chessboard metasurfaces. Each unit cell is composed of an ITO square patch, PET substrate and ITO backplane. By selecting the size and surface resistance of the ITO square patch of unit cells by OMEPC, the designed chessboard metasurface can achieve a 10 dB RCS reduction from 10.1 to 26.4 GHz. The designed metasurface is a single-layer structure with a total thickness of 2 mm. Compared with previous work, the designed chessboard metasurface has multiple advantages such as simple structure, smoothness, thinness, high transparency, and flexibility. The proposed metasurface has broad prospects for EM stealth in some special applications, such as aircraft cabins.

II. THEORY AND DESIGN

A. BASIC THEORY OF RCS REDUCTION

Fig.1 shows a multielement chessboard metasurface containing $P = M \times N$ supercells and is spaced d_x and d_y in the x and y directions, respectively. For a equal-sized

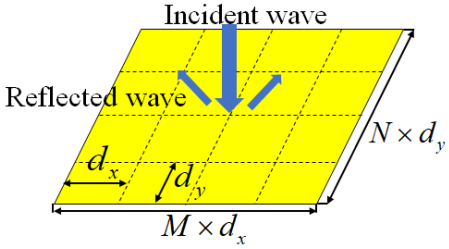

FIGURE 1. RCS reduction mechanism of a multielement chessboard metasurface.

perfect electric conductor (PEC) surface, the maximum backscattering field is generated under normal incidence. But for the metasurface in Fig.1, reflected waves from different supercells interfere at the same spatial location, causing the backscattering field to deviate from the incident direction. Compared with an equal-sized PEC surface, the RCS reduction of the metasurface under normal incidence can be approximated as [30]

$$\sigma_R = 20 \log \left| \frac{\sum_{m=1}^{M} \sum_{n=1}^{N} A_{m,n} e^{j\phi_{m,n}}}{M \times N} \right| \tag{1}$$

where $A_{m,n}$ and $\phi_{m,n}$ are the reflection amplitude and phase of the (m, n) supercell, respectively. Extensive calculations prove that when each supercell contains more unit cells, the estimation result of (1) is more accurate [30].

B. UNIT CELL DESIGN

In order to make the metasurface optically transparent, a square ITO patch etched on the PET substrate was selected as the basic unit cell, as shown in Fig.2a. ITO square films are designed with different surface resistances R_1 and side length d. The periodic size of super particles is $p = 8$ mm, and the spacing between ITO square patches is $s = p - d$. For different R_1 and d, unit cells have different reflection amplitudes and phases. The PET substrate has a fixed thickness of $h = 2$ mm and a relative permittivity of $\varepsilon_{PET} = 3$ [32]. To reduce the transmittance, the unit cell has an ITO backplane with a surface resistance of R_2. Fig.Fig.2b shows the equivalent circuit model (ECM) of the basic unit cell. The surface current of the ITO square patch generates inductance, and the accumulation of charges on the edge will generate capacitance, so it is equivalent to an RLC series circuit. The PET substrate is equivalent to a transmission line, and the ITO bottom plate is equivalent to a resistor. The circuit parameters can be calculated as [32]

$$\begin{aligned} R'_1 &= (p/d)^2 R_1, C'_1 = \varepsilon_0 \varepsilon_{eff} \frac{2p}{\pi} \ln(1/(\sin \frac{\pi s}{2p})) \\ L'_1 &= \mu_0 \frac{p}{2\pi} \ln(1/(\sin \frac{\pi d}{2p})), R'_2 = R_2 \end{aligned} \tag{2}$$

It can be deduced from ECM that when R_2 is smaller, the transmittance of the unit cell will be lower. When R_2 is 0 Ω/sq, the ITO backplane is equivalent to a perfect electrical conductor (PEC) surface, and all incident

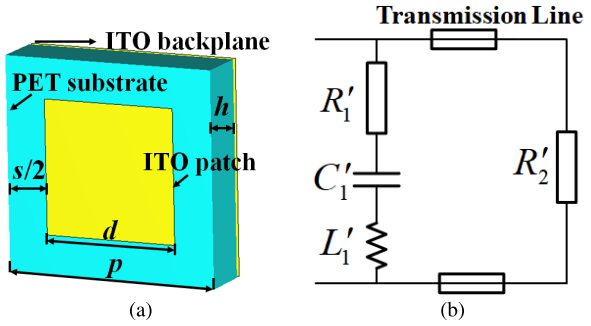

FIGURE 2. (a) Geometry of the basic unit cell. (b) Equivalent circuit model of the basic unit cells.

waves will be absorbed or reflected. Considering the actual processing, the surface resistance of the ITO backplane is determined to be 10 Ω/sq, which can make the transmittance of the unit cell lower than -20 dB. The side length d of ITO square films can vary from 1.6 to 7.6 mm with a step size of 0.2 mm. For convenience, three types of ITO patches with different surface resistances are selected, which are 10, 50 and 100 Ω/sq. Fig.3a-3b, 3c-3d and 3e-3f are the reflection amplitudes and phases of unit cells under different d when R_1 is 10, 50, and 100 Ω/sq, respectively. The simulation used the frequency domain solver of CST Studio Suite 2022 software. It can be seen the reflection amplitudes and phases change dramatically with the variation of R_1 and d. The absorption rate of unit cells can be calculated as $A = 1 - R^2$, where R is the reflection amplitude. It can be calculated that the 90% absorption bandwidth of unit cells at different R_1 and d is very narrow, which indicates that relying solely on the absorption effect is difficult to achieve 10 dB RCS reduction over a wide frequency band.

C. OPTIMIZATION DESIGN OF MULTIELEMENT METASURFACE

In this study, the designed metasurface consists of 4×4 supercells, and each supercell consists of 6×6 unit cells. The total size of the metasurface is 192 mm $\times$ 192 mm. The aim is to optimize the surface resistance R_1 and side length d of 16 types of unit cells to achieve the highest 10 dB RCS reduction bandwidth of the metasurface. Fig.4 shows the flowchart of RCS reduction optimization. The particle swarm optimization (PSO) method combined with (1) was used to optimize R_1 and d. The optimization frequency range is from 0.01 to 30 GHz, with an interval of 0.01 GHz, and a total of $Q = 3000$ frequency points. First, $P = 16$ combinations of R_1 and d are randomly selected. Then, the reflection amplitude and phase corresponding to the 16 combinations can be obtained. By using (1), the RCS reduction corresponding to 3000 frequency points can be calculated. Define the fitting function as

$$fitness = \sum_{i=1}^{Q} s(i),\ s(i) = \begin{cases} 1, if\ \sigma_R^i > -10dB \\ 0, if\ \sigma_R^i \le -10dB \end{cases} \quad (3)$$

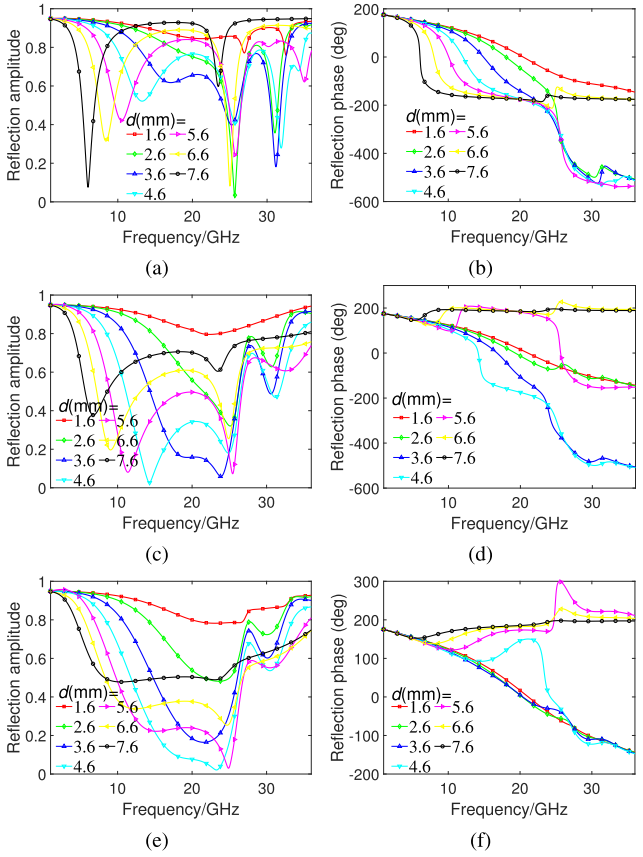

FIGURE 3. Reflection amplitudes and phases of unit cells at different R_1 and d. (a)-(b) $R_1 = 10\Omega/sq$. (c)-(d) $R_1 = 50\Omega/sq$. (e)-(f) $R_1 = 100\Omega/sq$.

The fitting function is used to count the number of σ_R^i greater than -10 dB. Therefore, the purpose of optimization is to achieve the minimum value of *fitness*. The final optimized chessboard configuration is shown in Fig.5, and the parameter values of R_1 and d corresponding to the index in Fig.5 are displayed in Table 1. Since the arrangement of 16 supercells has almost no effect on the RCS reduction under normal incidence, we arrange them in the initialization order [30].

TABLE 1. Optimized results of 16 unit cells.

array	1	2	3	4	5	6	7	8
$R_1(\Omega/sq)$	50	100	100	10	10	100	100	50
d(mm)	6.2	3	4.4	4.6	6.8	5.6	3.2	6.6
array	9	10	11	12	13	14	15	16
$R_1(\Omega/sq)$	100	10	10	100	50	100	10	50
d(mm)	3.4	6	6.4	5.8	5.6	6.4	5.8	3.2

III. SIMULATION AND MEASUREMENT

A sample of the proposed metasurface was fabricated, as shown in Fig.6a. First, 0.1 mm thick ITO-PET films with different surface resistances were obtained through

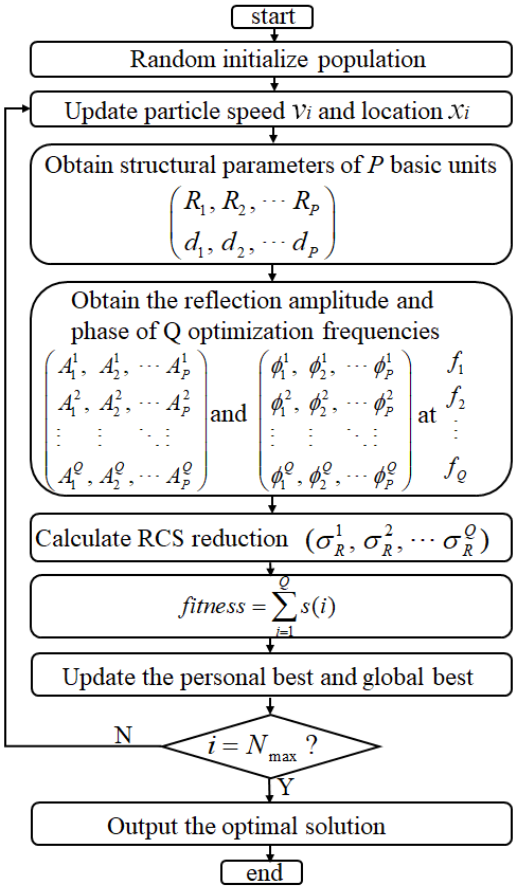

FIGURE 4. Flowchart of the unit cell optimization process.

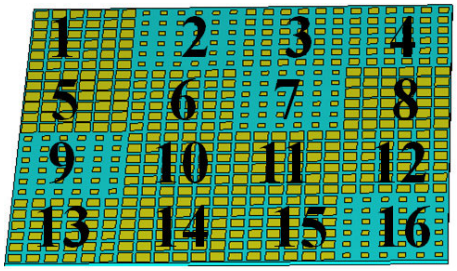

FIGURE 5. The metasurface model obtained after optimization. The inserted index is the supercell number shown in Table 1.

magnetron sputtering technology, where the thickness of ITO was all 180 nm. ITO square arrays were obtained through laser etching technology and then spliced together. Due to the thinness of ITO, it has almost no effect on the thickness of the entire structure. Finally, the upper ITO pattern film and lower ITO backplane were pasted to a 1.8 mm PET substrate through transparent glue. From Fig.6a, the image below the sample can be clearly seen. Since the total thickness of the sample is only 2 mm, it has good flexibility, as shown in Fig.6b. A UV/Vis/NIR spectrometer was used to measure the transmittance in the visible wavelength range of 400-800 nm. Multiple positions of the sample were measured, and Fig.Fig. 6c shows the average transmittance.

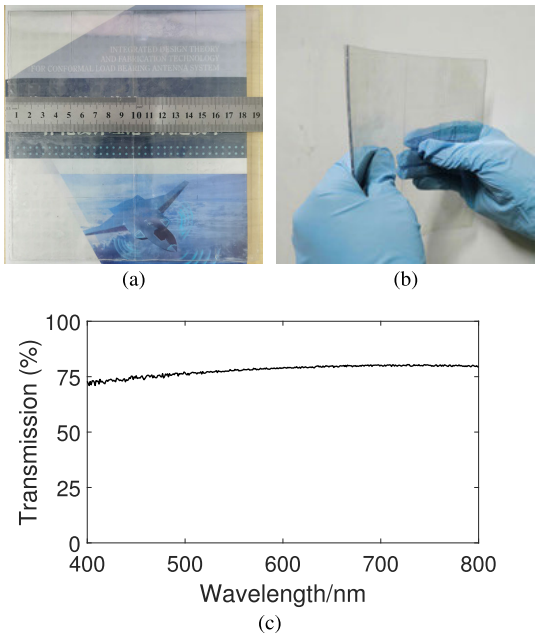

FIGURE 6. (a) Photograph of the fabricated sample. (b) The fabricated sample after bending. (c)The average transmittance of the fabricated sample in the visible light wavelength range of 400-800 nm.

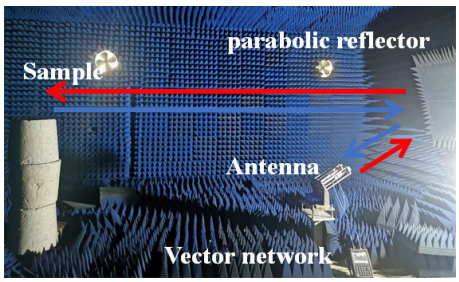

FIGURE 7. Experimental setup for RCS testing.

It can be seen that the transmittance of the sample in the visible light band is about 0.75, which proves the good optical transparency of the proposed metasurface.

The RCS of the sample was tested in a microwave darkroom, as shown in Fig.7. Two antennas were connected to a vector network analyzer (N9918A) through transmission lines. The total operating frequency range of the antenna is 8-26 GHz. The positions of the two antennas are fixed. The transmitting antenna generates incident waves, which are converted into plane waves by a parabolic reflector. The scattered waves from the sample are reflected by the parabolic reflector and then received by the receiving antenna. Fig.8 is the RCS reduction results obtained through (1), full-wave simulation and experiment, respectively. It can be seen that the results obtained by the three methods are in good agreement. The proposed metasurface can achieve 10 dB RCS reduction in the frequency range of 10.1-26.4 GHz. In addition, it can be seen that the metasurface has the largest RCS reduction value when the incident frequency is 25 GHz. This is mainly because the unit cells that make

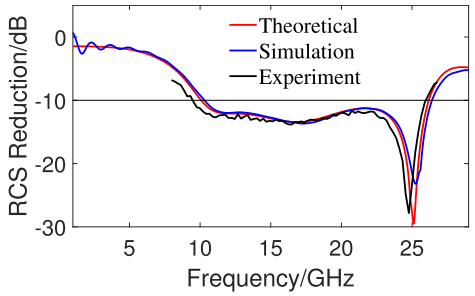

FIGURE 8. RCS reduction results obtained through theoretical analysis by (1), full wave simulation, and experimental measurement.

up the metasurface have a large absorption rate at 25 GHz. Therefore, the RCS reduction of the proposed metasurface is the result of a combination of wave absorption and reflection phase interference.

To further reveal the RCS reduction mechanism of the designed metasurface, the corresponding energy dissipation ratio under normal incidence can be calculated as [29]

$$\begin{aligned} A(\omega) &= \sum_{m=1}^{M}\sum_{n=1}^{N}(1-A_{m,n}^2)/(M\times N) \\ PC(\omega) &= \left|\sum_{m=1}^{M}\sum_{n=1}^{N}A_{m,n}e^{j\phi_{m,n}}/(M\times N)\right|^2 \\ R(\omega) &= 1-A(\omega)-PC(\omega) \end{aligned} \tag{4}$$

where $A(\omega)$, $PC(\omega)$, and $R(\omega)$ represent the energy ratio of absorption, phase interference, and reflection, respectively. $A_{m,n}$ and $\phi_{m,n}$ in (4) were obtained through CST simulation.

When the sum of $A(\omega)$ and $PC(\omega)$ exceeds 90%, $R(\omega)$ will be lower than 10%, and the RCS reduction will be greater than 10 dB [25]. Fig.9 shows the proportion of energy distribution at different incident frequencies. It can be seen that both absorption and phase interference play important roles in RCS reduction, and the broadband scattering reduction is the result of the combination of these two effects.

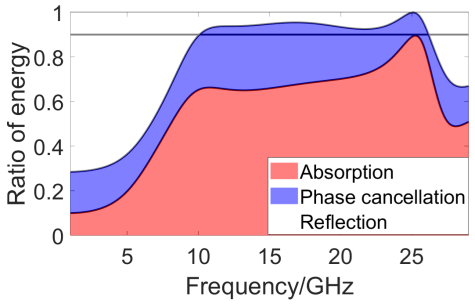

FIGURE 9. The energy ratio of absorption, phase interference, and reflection of the designed metasurface.

Fig.10a-10d shows the 3D RCS patterns of the proposed metasurface and an equal-sized PEC surface under normal incidence at 15 and 25 GHz, respectively. It can be clearly seen that the scattering lobe of the PEC surface are concentrated in the normal incident direction, while multiple scattering lobes are spread at multiple directions around

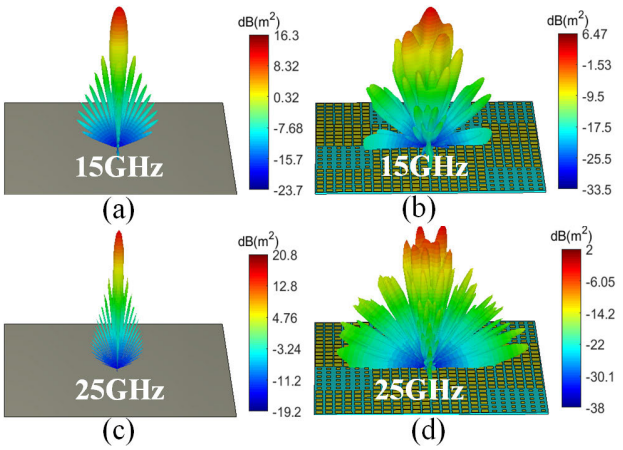

FIGURE 10. Comparison of the scattering patterns of the proposed metasurface and an equal-sized PEC surface under normal incidence at (a)-(b) 15 GHz and (c)-(d) 25 GHz.

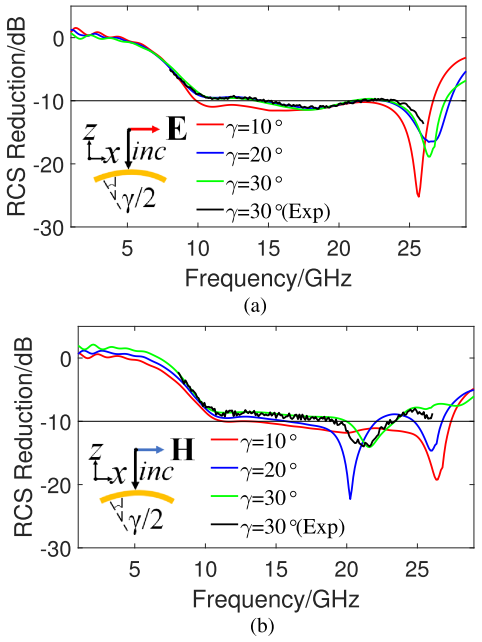

FIGURE 11. RCS reduction of the designed metasurface at different curvature angles γ and polarizations. (a)TM polarization. (b)TE polarization.

the metasuface. In addition, the proposed metasurface has an absorbing effect, so the scattering in the normal incidence direction is lower than that of the PEC surface.

Due to the extremely low thickness of the designed metasurface, it can be appropriately curved. Here, a cylindrical bending is performed on the metasurface with a curvature angle of γ. Fig. 11 shows the RCS reduction simulated by CST under different polarizations when γ is 10°, 20°, and 30°, respectively. It can be seen that the performance of the metasurface slightly decreases after bending, but it still has a RCS reduction effect of nearly 10 dB in the frequency range of 10-25 GHz. The main reason for the decrease in RCS reduction effect is that bending affects the impedance matching. The fabricated sample is bent

TABLE 2. Comparison of the proposed chessboard metasurface with some previously reported structures.

Ref	OFB(GHz)	RBW(%)	Thickness(mm)/λ_L	Optical transparency	Flexibility	Number of layers	Mechanism
[21]	25-37.8	40	0.8/0.032λ_L	/	No	1	Phase Cancellation
[22]	3.9-9.5	83	6.35/0.082λ_L	/	No	1	Phase Cancellation
[30]	5.5–32.3	141	6/0.11λ_L	/	No	1	Phase Cancellation
[31]	6.5–64.8	163	6/0.13λ_L	/	No	1	Phase Cancellation
[32]	12.5–98.2	154.9	4.2/0.17λ_L	60.49%	No	2	Absorption
[33]	6.2–20.8	108	3/0.062λ_L	77%	Yes	1	Hybrid Mechanism
[35]	7–18.2	88.9	3.35/0.078λ_L	60%	No	2	Absorption
[36]	7.5–32.2	124.5	4/0.1λ_L	55%	No	2	Hybrid Mechanism
This work	10.1-26.4	89	2/0.067λ_L	75%	Yes	1	Hybrid Mechanism

OFB:Operating frequency of the 10 dB RCS reduction. RBW:Relative bandwidth of OFB. λ_L:Wavelength corresponding to the lowest frequency of 10 dB RCS reduction.

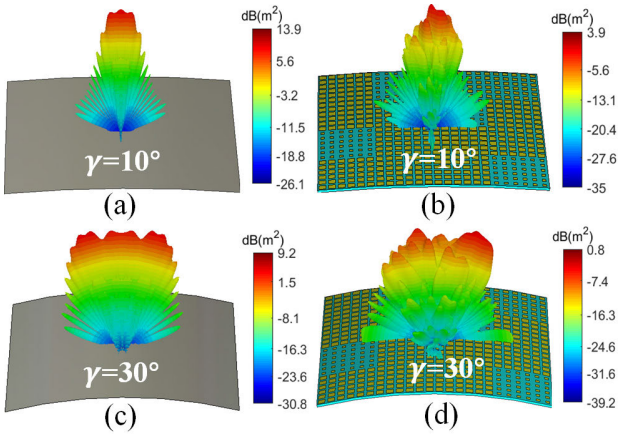

FIGURE 12. Comparison of the scattering patterns of the proposed metasurface and an equal-sized PEC surface at (a)-(b) γ=10° and (c)-(d) γ=30°.

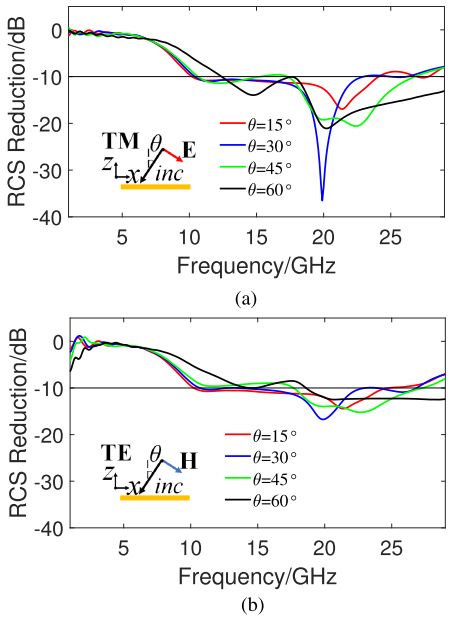

FIGURE 13. RCS reduction in the specular direction under different oblique incidence angles and polarizations. (a)TM polarization. (b)TE polarization.

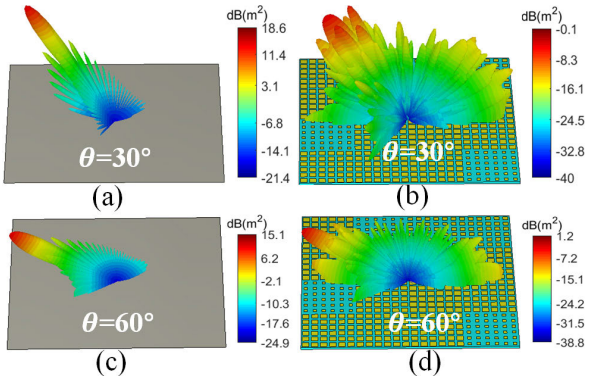

FIGURE 14. Comparison of the scattering patterns of the proposed metasurface and an equal-sized PEC surface at (a)-(b) θ=30° and (c)-(d) θ=60°.

with a curvature angle of 30° and tested experimentally. The experimental results are basically consistent with the simulation results. Fig.12 shows the 3D RCS modes of the proposed metasurface and an equal-sized PEC at γ values of 10° and 30°, respectively. At this time, the incident frequency is 20 GHz and the polarization mode is TM polarization. It can be seen that as γ increases, the scattered lobes concentrate in more directions. Meanwhile, due to the asymmetry of the metasurface, the scattering lobes are also asymmetric. The scattering of metasurfaces in the normal incidence direction is still much lower than that of PEC surface.

Fig. 13 shows the RCS reduction simulated by CST in the specular direction of the proposed metasurface at oblique incidence angles of 15°, 30°, 45° and 60° under TE and TM polarization. It can be seen that the metasurface can still achieve nearly 10 dB RCS reduction nearly 10 dB in the frequency range of 10-25 GHz when the incidence angle is less than 45°, indicating that the proposed metasurface has good polarization and angular stability. Furthermore, it can be observed that the incident angle stability under TM polarization is higher than that under TE polarization. The reason for the difference is that different polarizations generate different wave impedances, leading to different impedance matching and absorption of incident waves. Fig.14 shows the 3D RCS modes of the proposed metasurface and an equal-sized PEC at oblique incidence angles of 30°

and 60°, respectively. The incident frequency is 20 GHz and the polarization mode is TM polarization. Similar to the situation under normal incidence, the metasurface exhibits multiple lobes under oblique incidence, and the RCS in the specular direction is much lower than that of the PEC surface.

Table 2 compares the proposed metasurfaces with some published works. It can be seen that although the proposed metasurface does not have outstanding advantages in 10 dB RCS reduction bandwidth, it has unparalleled advantages of optical transparency and flexibility. Meanwhile, the metasurface is a single-layer structure and have an extremely low thickness of 2mm, which is far lower than the thickness of other flexible and transparent metasurfaces. Therefore, the proposed metasurface has stronger practicality and great potential for some special applications such as stealth aircraft canopy.

IV. CONCLUSION

In this paper, A multielement single-layer chessboard metasurface with simultaneously optical transparency, flexibility, and broadband RCS reduction is designed, manufactured, and tested. The metasurface are composed of ITO square films, PET substrate, and an ITO backplane. By optimizing the surface resistance and side length of unit cells through the OMEPC method, the proposed metasurface can achieve a 10 dB RCS reduction from 10.1 to 26.4 GHz with a relative bandwidth of 89% under normal incidence. The total thickness of the metasurface is only 2 mm, which makes it highly flexible. Theoretical analysis, simulations, and experimental tests have all demonstrated the excellent characteristics of the proposed metasurface. In summary, this work has great prospects in some special application of stealth, such as aircraft canopy and stealth glass.

REFERENCES

[1] W. Li, M. Xu, H. Xu, X. Wang, and W. Huang, "Metamaterial absorbers: From tunable surface to structural transformation," *Adv. Mater.*, vol. 34, no. 38, Sep. 2022, Art. no. e2202509.

[2] Q. Chang, W. Wu, Y. Ma, X. Ji, and J. Ji, "Transparent and tunable water-based metamaterial absorber with low infrared emissivity," *Appl. Phys. Lett.*, vol. 123, no. 7, Aug. 2023, Art. no. 071702.

[3] M. Heidari, S. H. Sedighy, and M. K. Amirhosseini, "RCS reduction using grounded multi-height multi-dielectrics metasurfaces," *Sci. Rep.*, vol. 13, no. 1, p. 3069, Feb. 2023.

[4] Z. Zhang, Y. Zhou, T. Li, S. Li, H. Yang, J. Tian, and X. Cao, "Low-profile shared-aperture metasurface array antenna with ultra-wideband radar cross section reduction and circularly polarization," *J. Appl. Phys.*, vol. 134, no. 11, Sep. 2023, Art. no. 115101.

[5] Q. Chang, Y. Ma, J. Liu, W. Wu, X. Ji, and J. Ji, "Equivalent circuit model for reflective polarization converter based on anisotropic metasurfaces," *J. Appl. Phys.*, vol. 132, no. 7, Aug. 2022, Art. no. 073101.

[6] C. Wang, R.-Z. Wang, S.-J. Zhang, H. Wang, and W.-S. Wang, "Reducing radar cross section of flat metallic targets using checkerboard metasurface: Design, analysis, and realization," *J. Appl. Phys.*, vol. 134, no. 4, Jul. 2023, Art. no. 044902.

[7] C. F. Zhou, Q. F. Yu, C. Gustafson, and B. K. Lau, "Wideband RCS reduction based on a simple chessboard metasurface," *J. Appl. Phys.*, vol. 133, no. 18, May 2023, Art. no. 185302.

[8] B. Lin, W. Huang, L. Lv, J. Guo, Z. Liu, and R. Zhu, "An ultra-wideband circular polarization-maintaining metasurface and its application in RCS reduction," *IEEE Access*, vol. 9, pp. 103967–103974, 2021.

[9] H. Takeshita, D. Nita, Y. Cheng, A. A. Fathnan, and H. Wakatsuchi, "Dual-band waveform-selective metasurfaces for reflection suppression," *Appl. Phys. Lett.*, vol. 123, no. 19, Nov. 2023, Art. no. 191703.

[10] P. Tiwari, S. K. Pathak, and V. Siju, "Design, development and characterization of resistive arm based planar and conformal metasurfaces for RCS reduction," *Sci. Rep.*, vol. 12, no. 1, p. 14992, Sep. 2022.

[11] J. Chatterjee, A. Mohan, and V. Dixit, "Ultrawideband RCS reduction of planar and conformal surfaces using ultrathin polarization conversion metasurface," *IEEE Access*, vol. 10, pp. 36563–36575, 2022.

[12] Y. Lu, J. Su, J. Liu, Q. Guo, H. Yin, Z. Li, and J. Song, "Ultrawideband monostatic and bistatic RCS reductions for both copolarization and cross polarization based on polarization conversion and destructive interference," *IEEE Trans. Antennas Propag.*, vol. 67, no. 7, pp. 4936–4941, Jul. 2019.

[13] Z. Ren, Y. Q. Liu, Y. Wang, L. Lu, K. Qi, and H. Yin, "Ultra-broadband RCS reduction based on optimized coding 'whale-shaped' polarization conversion metasurface with angular stability," *IEEE Access*, vol. 10, pp. 50479–50486, 2022.

[14] G.-Y. Deng, Y.-H. Zhang, S.-Y. He, H. Yan, H.-C. Yin, H.-T. Gao, and G.-Q. Zhu, "Ultrabroadband RCS reduction design by exploiting characteristic complementary polarization conversion metasurfaces," *IEEE Trans. Antennas Propag.*, vol. 70, no. 4, pp. 2904–2914, Apr. 2022.

[15] F. Li and B. You, "Complementary multi-band dual polarization conversion metasurface and its RCS reduction application," *Electronics*, vol. 11, no. 10, p. 1645, May 2022.

[16] R. Wu, S. Cao, Y. Liu, and S. Cai, "A wideband low-profile dual-polarized antenna based on a metasurface," *Electronics*, vol. 12, no. 23, p. 4739, Nov. 2023.

[17] M. K. T. Al-Nuaimi, W. G. Whittow, G.-L. Huang, R.-S. Chen, and Q. Shao, "Hybrid cubic-chessboard metasurfaces for wideband angle-independent diffusive scattering and enhanced stealth," *Opt. Exp.*, vol. 31, no. 24, pp. 39433–39446, 2023.

[18] W. Chen, C. A. Balanis, and C. R. Birtcher, "Dual wide-band checkerboard surfaces for radar cross section reduction," *IEEE Trans. Antennas Propag.*, vol. 64, no. 9, pp. 4133–4138, Sep. 2016.

[19] D. Sang, Q. Chen, L. Ding, M. Guo, and Y. Fu, "Design of checkerboard AMC structure for wideband RCS reduction," *IEEE Trans. Antennas Propag.*, vol. 67, no. 4, pp. 2604–2612, Apr. 2019.

[20] S. A. M. Soliman, E. M. El-Desouki, S. M. El-Nady, and A. S. A. El-Hameed, "Broadband low RCS based on polarization—Dependent artificial magnetic conductor metasurface," *IEEE Access*, vol. 11, pp. 53176–53184, 2023.

[21] M. F. El-Sewedy and M. A. Abdalla, "A monostatic and bistatic RCS reduction using artificial magnetic conductor metasurface," *IEEE Trans. Antennas Propag.*, vol. 71, no. 2, pp. 1988–1992, Feb. 2023.

[22] A. Y. Modi, C. A. Balanis, C. R. Birtcher, and H. N. Shaman, "Novel design of ultrabroadband radar cross section reduction surfaces using artificial magnetic conductors," *IEEE Trans. Antennas Propag.*, vol. 65, no. 10, pp. 5406–5417, Oct. 2017.

[23] Z. Zhao, X. Li, and G. Dong, "Wideband RCS reduction based on hybrid checkerboard metasurface," *Sensors*, vol. 23, no. 8, p. 4054, Apr. 2023.

[24] B. Bandyopadhyay, S. Bhattacharya, R. K. Jaiswal, M. Saikia, and K. V. Srivastava, "Wideband RCS reduction of a linear patch antenna array using AMC metasurface for stealth applications," *IEEE Access*, vol. 11, pp. 127458–127467, 2023.

[25] W. Chen, C. A. Balanis, and C. R. Birtcher, "Checkerboard EBG surfaces for wideband radar cross section reduction," *IEEE Trans. Antennas Propag.*, vol. 63, no. 6, pp. 2636–2645, Jun. 2015.

[26] G.-S. Huang, S.-J. Li, Z.-Y. Li, X.-B. Liu, C.-Y. He, H.-H. Yang, and X.-Y. Cao, "Multifunctional coding-feeding metasurface based on phase manipulation," *Materials*, vol. 15, no. 19, p. 7031, Oct. 2022.

[27] M. Moccia, S. Liu, R. Y. Wu, G. Castaldi, A. Andreone, T. J. Cui, and V. Galdi, "Coding metasurfaces for diffuse scattering: Scaling laws, bounds, and suboptimal design," *Adv. Opt. Mater.*, vol. 5, no. 19, Oct. 2017, Art. no. 1700455.

[28] M. K. T. Al-Nuaimi and W. G. Whittow, "Design of QR-coded metasurfaces for RCS reduction at mmWave," *IEEE Access*, vol. 10, pp. 66267–66272, 2022.

[29] J. Su, Y. Li, M. Qu, H. Yu, Q. Guo, and Z. Li, "A 3-D-printed ultrawideband and ultralow-scattering water-based metasurface," *IEEE Trans. Antennas Propag.*, vol. 71, no. 3, pp. 2885–2890, Mar. 2023.

[30] J. Su, Y. Lu, J. Liu, Y. Yang, Z. Li, and J. Song, "A novel checkerboard metasurface based on optimized multielement phase cancellation for superwideband RCS reduction," *IEEE Trans. Antennas Propag.*, vol. 66, no. 12, pp. 7091–7099, Dec. 2018.
[31] M. Qu, C. Zhang, J. Su, J. Liu, and Z. Li, "Extremely wideband and omnidirectional RCS reduction for wide-angle oblique incidence," *IEEE Trans. Antennas Propag.*, vol. 70, no. 8, pp. 7288–7293, Aug. 2022.
[32] J. Ge, Y. Zhang, H. Li, H. Dong, and L. Zhang, "Ultra-broadband, tunable, and transparent microwave meta-absorber using ITO and water substrate," *Adv. Opt. Mater.*, vol. 11, no. 10, May 2023, Art. no. 2202873.
[33] S. Sui, J. Wang, Y. Pang, J. Zhang, Z. Xu, and S. Qu, "Transparent metasurface for wideband backward scattering reduction with synthetic optimization algorithm," *J. Phys. D, Appl. Phys.*, vol. 55, no. 27, Jul. 2022, Art. no. 275002.
[34] Q. Chang, J. Ji, W. Wu, and Y. Ma, "An optically transparent metamaterial absorber with tunable absorption bandwidth and low infrared emissivity," *Materials*, vol. 16, no. 23, p. 7357, Nov. 2023.
[35] J. Zhang, Z. Li, L. Shao, and W. Zhu, "Dynamical absorption manipulation in a graphene-based optically transparent and flexible metasurface," *Carbon*, vol. 176, pp. 374–382, May 2021.
[36] Y. Xi, W. Jiang, K. Wei, T. Hong, and S. Gong, "An optically transparent hybrid mechanism metasurface for wideband, wide-angle and omnidirectional scattering suppression," *IEEE Trans. Antennas Propag.*, vol. 71, no. 1, pp. 422–432, Jan. 2023.

QI CHANG received the M.S. degree in engineering from Beihang University, Beijing, China, in 2021, where he is currently pursuing the Ph.D. degree in aeronautical engineering. His current research interests include computational electromagnetics and the design of metamaterials.

JINZU JI received the B.S. and Ph.D. degrees in engineering from Beihang University, Beijing, China, in 2005 and 2009, respectively.

He is currently a Professor with Beihang University. He has authored or coauthored more than 40 articles about computational electromagnetics. His current research interests include the study of computational electromagnetics, plasma behavior simulation, and particularly finite-different time-domain.

YUNPENG MA received the B.S. and Ph.D. degrees in engineering from Beihang University, Beijing, China, in 2005 and 2010, respectively.

He is currently a Professor with Beihang University. His research interests include computational electromagnetics and stealth technology.